PCCP

Theoretical Studies on the energy structures and optical properties of Copper Cysteamine – A Novel Sensitizer

Journal:	*Physical Chemistry Chemical Physics*
Manuscript ID	CP-ART-08-2019-004392
Article Type:	Paper
Date Submitted by the Author:	08-Aug-2019
Complete List of Authors:	Alias, Marc; Universitat Rovira i Virgili Alkhaldi, Noura ; University of Texas at Arlington Reguero, Mar; Universitat Rovira i Virgili, Química Física i Inorgànica Ma, Lun; University of Texas at Arlington, Department of physics Zhang, Junying; Beihang University, Graaf, Coen; Universitat Rovira i Virgili Huda, Muhammad; University of Texas at Arlington, Physics Chen, Wei; The University of Texas, Department of Physics

Theoretical Studies on the energy structures and optical properties of Copper Cysteamine – A Novel Sensitizer

Marc Alias,[1] Noura D. Alkhaldi,[2] Mar Reguero,*[1] Lun Ma,[2] Junying Zhang,[3] Coen de Graaf,[1,4] Muhammad N. Huda*[2] and Wei Chen*[2]

[1] Departament de Química Física i Inorgànica, Universitat Rovira i Virgili, 43007, Tarragona, Spain

[2] Department of Physics, The University of Texas at Arlington, Arlington, Texas 76019-0059, USA

[3] Department of Physics, Beihang University, Beijing 100191, China

[4] ICREA, Pg. Lluís Companys 23, 08010, Barcelona, Spain

Corresponding authors: weichen@uta.edu; mar.reguero@urv.cat; huda@uta.edu

Abstract: Copper cysteamine (Cu-Cy) is a new type of photosensitizer, which can be activated not only by ultraviolet light, but also by X-rays, microwaves and ultrasound to generate reactive oxygen species for treating cancer and infection diseases. Moreover, copper cysteamine has a strong luminescence which can be used for both therapeutics and imaging. In addition, it also can be used for solid state lighting, radiation detection and sensors. However, its electronic structures, and particularly its excited states, are not yet clear. Here, we present a computational study aimed to determine the nature of the excited states involved in the photophysical processes that give place to the luminescence of this compound. The study has been conducted using density functional theory (DFT), using both hybrid functionals and time-dependent DFT. It is found that both absorption and emission involve the replacement of an electron among the 3d and 4s orbitals of one or the other of the two types of Cu atoms found in the system. Our computed results compared well with the experimental absorption and emission results. These results are very helpful for the understanding of the experimental observations.

Key Words: Copper cysteamine, excited states, density functional theory, optical absorption, luminescence, triplet state, decay lifetime

1. Introduction

Copper is one of the transition metals often found in living organisms, both in its reduced and oxidized forms.[1, 2] It is an essential trace element and its imbalances are associated with various pathological conditions, including cancer, albeit via largely undefined molecular and cellular mechanisms.[1, 3] Being a soft Lewis acid by the HSAB (hard-soft acid-base) classification of Pearson, [4] Cu(I) can be found in enzymes and proteins bound to sulphur-containing amino acids, while the oxidized form, Cu(II), is typically coordinated by the harder N atoms. Binuclear (or polynuclear) Cu(I) compounds often show a short Cu-Cu distance in the range of the sum of Van der Waals radii, a property known as "cuprophilicity".[1]

Copper complexes have been widely studied as anticancer drugs.[1-4] The presence of elevated levels of copper and oxidative stress in cancer patients compared to normal subjects has been well documented. The elevated copper and oxidative stress levels are hallmarks of a range of malignancies, and so the control of these levels provides approaches to treatments that are applicable to a variety of malignant conditions.[5] Copper causes oxidative stress in cancer cells by reactive oxygen species (ROS) produced through metal catalyzed oxidation, resulting in cell death.[6, 7] For this reason, the application of established copper chelators, such as D-Penicillamine (D-pen), are applied as anticancer agents. Angiogenesis, the formation of new capillaries from existing vasculature, is a critical process in normal physiology as well as in several physiopathologies. A desire to curb the supportive role that angiogenesis plays in the development and metastasis of cancers has driven to the exploration of anti-angiogenic strategies such as cancer therapeutics. It has been reported that copper ions are closely related to angiogenesis in tumors, so chelation of copper ions is also a good method to inhibit angiogenesis and cancer progression.[8, 9] For these reasons, the development of anti-cancer agents that target the altered copper and oxidative stress conditions in malignancies are potentially good solutions to stop cancers.[5, 6 8, 9]

There is an enormous variety of ligands that can be connected to copper. One of them is Cysteamine (Cy), otherwise expressed as 2-amino-ethanethiol ($HSCH_2CH_2NH_2$). Cysteamine is a small organic molecule that is formed in the degradation of cysteine, an amino acid. It can be incorporated in the metal coordination sphere by thiol or amino groups which provide Cy with a strong metal affinity.[1] Copper compounds have been largely studied because they are considered as model compounds of some enzymes with copper-sulfur bonds.[6] These compounds show different crystal structures depending on reaction conditions.[6] Recently, a new type of copper compound, copper cysteamine (Cu-Cy) crystal $Cu_3Cl(SR)_2$ ($R=CH_2CH_2NH_2$), has been synthesized by Chen's group [10] that crystallizes rapidly at high temperature. The structure of the new compound is quite different from the ones previously obtained, showing a simpler structure with both amino and thiol groups bound to two different types of copper ions labelled as Cu(1) and Cu(2).[10] This new Cu-Cy complex shows some characteristics that makes it especially interesting for cancer photodynamic therapy to treat cancers [10-18] and infection diseases.[19] First, it presents intense luminescence when irradiated by X-ray or light. Second, it is an effective photosensitizer of singlet oxygen when activated by ultraviolet light,[10, 15] X-rays[11, 14, 17, 18],

microwaves[12] or ultrasound.[16] This means that this compound can be used for treating tumors located both shallowly and deeply due to the higher penetration power of the X-ray, microwave or ultrasound wavelengths in comparison with visible light. Cu-Cy nanoparticles interact with X-rays, and produce both fluorescence[10] and singlet oxygen.[11] Singlet oxygen is a reactive oxygen species, which causes damage to cells. The mechanism for x-ray interactions with Cu-Cy nanoparticles to produce singlet oxygen is similar to the process for light activation to produce singlet oxygen; the only difference is that the excitation with x-rays is to higher excited levels, while the relaxation to lower energy levels and the energy transfer from the triplet state to excite dioxygen to produce oxygen are the same as in the regular light activation processes as addressed in our recent paper.[18] In addition, Cu-Cy can be activated by microwave [12] and ultrasound [16] to produce singlet oxygen and other reactive oxygen species (ROS) for cancer destruction. Under stimulation by these low energy electromagnetic waves, the major mechanism for ROS is the Fenton Reaction induced by Cu^+ released from Cu-Cy nanoparticles in tumor acidic environments, as revealed by Electron Spin Resonance (ESR) measurements in our previous publication.[12]

The characterization of the excited states involved in the phenomena that manifest above interesting properties is still largely unexplored. A detailed knowledge of these electronic states could help in the understanding of Cu-Cy and in the design of new compounds with specific characteristics. Computational chemistry is a very useful tool to elucidate the answers to these questions. This paper presents a computational study to determine the nature of the excited structures involved in the absorbance and luminescence of this Cu-Cy system. The study has been performed using density functional theory (DFT).[20-22] It is found that both absorption and emission involve the replacement of electrons among orbitals largely localized on copper atoms. The double emission feature at lower energy was found to arise from the two different copper sites in the unit cell of the compound within triplet state.

2. Computational details

The crystal structure and optical properties of Cu-Cy have been reported in our previous publication.[10] To understand the selection of the unit cell for the theoretical calculations, the packing diagram of Cu-Cy viewed along (001) (A) and the depiction of one strand as part of the unit cell are shown in **Figure 1**. The infinite 2-dimensional layers are linked by N(H)---Cl contact bonds, and is displayed in **Figure 2**. The inter layer bonds are very weak, Van der Waals type bonds. These structural data were used for the selection of the unit cells for the present computational study to determine the nature of the excited states involved in the photophysical processes of Cu-Cy system. The compound crystallizes in the monoclinic system in the space group C2/c. The unit cell shows two different types of Cu atoms: Cu(1), which is coordinated by two sulfur atoms and a Cl, and Cu(2), which binds to 4 other atoms in the crystal, three sulfurs and one N.

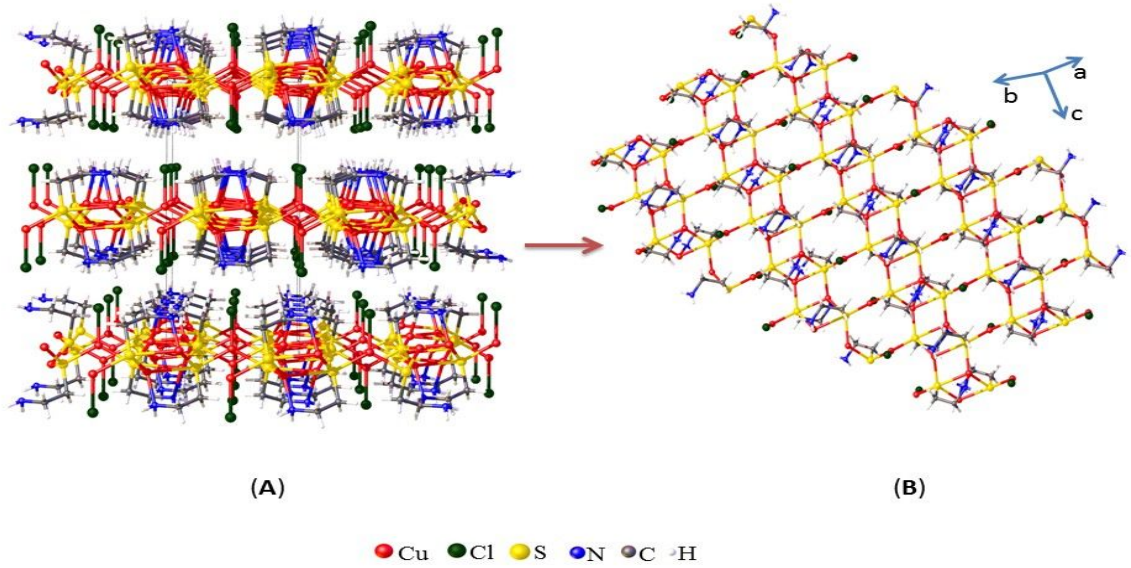

Figure 1. (A) Packing diagram of (1) viewed along (001). (B) Depiction of one strand as part of the unit cell.

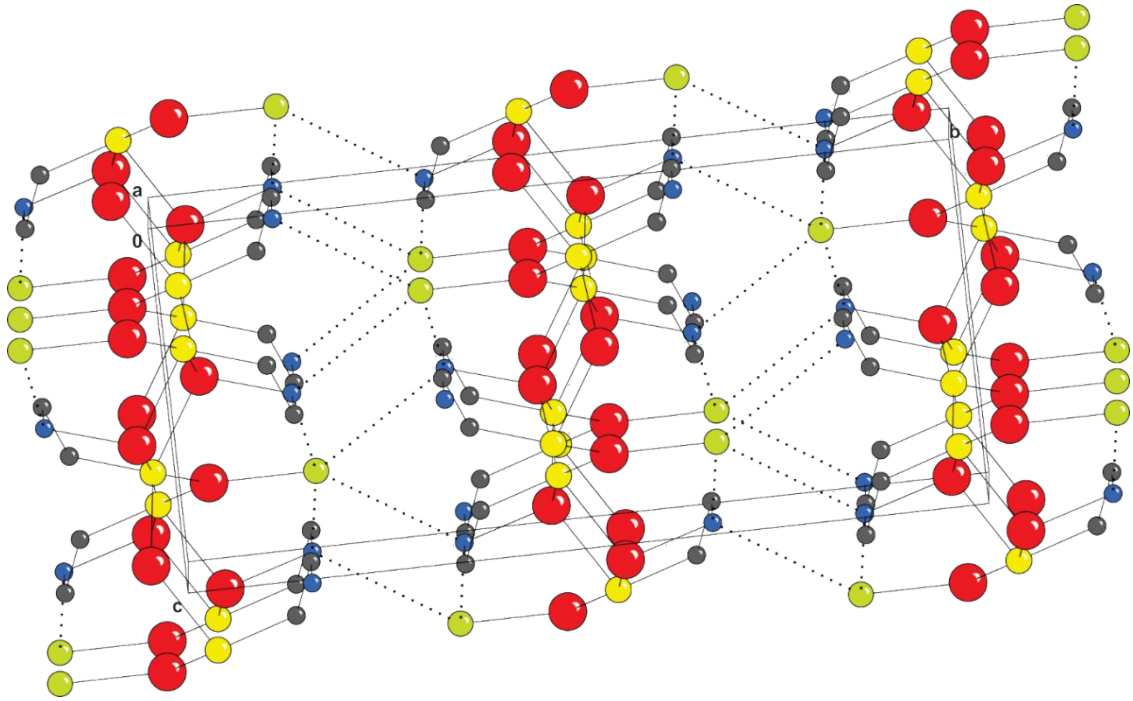

Figure 2. Infinite 2-dimensional networks are linked by N(H)---Cl contact bonds.

There are basically two methods to model Cu-Cy material. One method makes use of the translational symmetry of the theoretically perfect crystal, and the second one takes a local viewpoint and treats a small portion of the crystal (the cluster) in great detail. In the first approach, one can calculate the band structure of the system without making significant approximations in the representation of the material structure. The lowest unoccupied bands can be related to the lower-lying excited states. As the experimentally synthesized Cu-Cy was crystalline material, considering the translational symmetry with periodic boundary condition will

be a better representation of the experimental results. However, Cu-Cy is a molecular solid. So, care must be taken as the traditional DFT band structure calculations will intrinsically delocalize the band over the crystal layers and thus may not give an optimal description of the electronic states involved in the luminescence process, which can be locally excited states. To avoid some of these limitations we used hybrid functionals, HSE06, with Van der Waals corrections. However, in any case, the computational methods applicable to the system to be studied here, can provide accurate information only about the lowest state of each spin symmetry, i. e., S_0 and T_1, as Time dependent perturbation density functional theory for this large unite cell can be computationally too expensive. For this reason, we adopt the cluster model approach to represent the material as well. In this approach the region of interest where the excitation takes place is treated with the highest computational precision available, while the remainder of the crystal is represented in a less rigorous manner, yet accurate enough to provide a correct embedding of the 'chromophore'. Afterwards, the information obtained in this way is complemented with the one provided by the computations performed on a periodic model.

The cluster model that was used in the calculations consisted of the structural unit shown in **Figure 3**, extended with cysteamine and thioether groups on the Cu ions on the outside of the cluster, in which we embed the bare model in a set of pseudopotentials representing the Cu ions around the cluster. These pseudopotentials provide both the first (and largest) term of the electrostatic interaction due to the crystal on the cluster atoms, and a repulsive interaction to avoid an artificial delocalization of the electron density outside the cluster region. The position of these pseudopotentials was kept fixed in the geometry optimizations. The total charge of this model is +2.

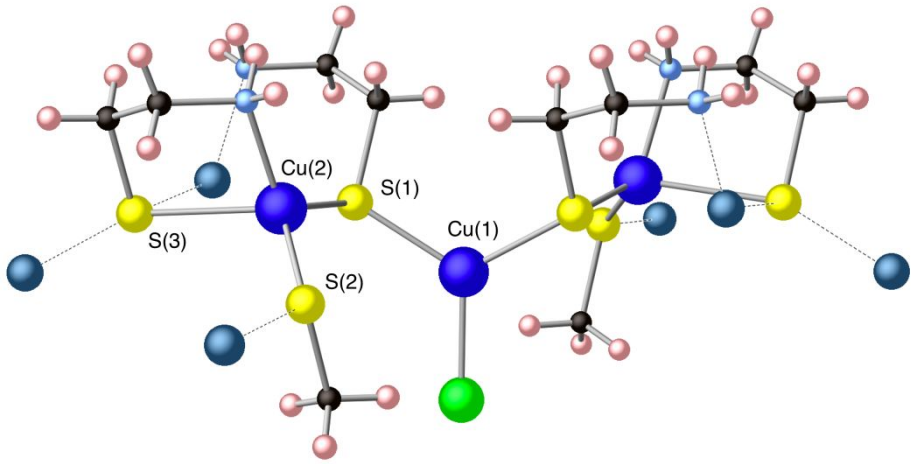

Figure 3. Ball and stick representation of the structural unit of the Cu-Cysteamine crystal. Cluster model used to estimate absorption and emission energies of the copper-cysteamine compound. Cl atoms are represented in green, S in yellow, Cu in dark blue, C in black, N in light blue and H in pink. The blue-grey spheres represent Cu pseudopotentials.

Geometry optimizations and energy calculations for the lowest energy states of each spin symmetry (S_0 and T_1 for the singlet and triplet manifolds, respectively) for the cluster model were performed using the Density Functional Theory (DFT) as implemented in Gaussian 09.[23] Time Dependent DFT (TD-DFT) with the Tamm-Dancoff approximation [20] was used to calculate the higher energy states of singlet and triplet multiplicity at the optimized geometries for the S_0 and T_1 states. Three different functionals have been tested: CAM-B3LYP [24], B3LYP [25] and PBE0 [26]. All calculations have been performed within the abelian C_2 point group symmetry. Two different basis sets have been used. Geometry optimizations were performed with Ahlrichs' split valence basis set with polarization (def2-SVP) for all atoms except for the ghost copper atoms, where the LANL2 pseudopotential was applied. At the located critical points, energies were recalculated using Ahlrichs' quadruple zeta basis set with polarization (def2-QZVP) for the all-electron atoms and LANL2 for the Cu^+ pseudopotentials.

Spin-orbit coupling (SOC) has been computed at the optimized T_1 state geometry by means of the Complete Active Space Self Consistent Field (CASSCF) method, with a minimal active space formed by 2 electrons in 2 active orbitals, CAS(2,2) and using the effective one-electron operator in the spin-orbit state interaction.

For the periodic system, calculations of this work such as relaxed bond-lengths and density of states at singlet and triplet states, optical absorptions coefficients, were done within the framework of density functional theory (DFT) as in Vienna ab initio simulation package (VASP).[21, 22, 27] We have utilized the Projector augmented-wave method (PAW) [28] and Heyd–Scuseria–Ernzerhof (HSE06) hybrid functional.[29] We relaxed all the structures before the total energies' calculation. As mentioned earlier, the inter-layer interactions are of the Van der Waals type, so for proper structural relaxations and total energy calculations for Cu-Cy, we included Van der Waals forces with the DFT Hamiltonian.[30]

3. Results and discussion

The discussion of the results is divided in three different parts. In the first one, we compare the lowest energy geometries of the S_0 and T_1 states obtained using the three different functions used in this work. The optimized S_0 geometry corresponds to the ground state structure of the Cu-Cy complex and can be compared with the experimental structure to check the accuracy of the computational set-up. In the second part, emission and absorption energies are calculated and compared with the available experimental data. The density functional that best reproduces the experimental results has been used in the final part to analyze the character of the excited states responsible for the emission and absorption observed experimentally.

3.1 Optimized geometries

From a theoretical point of view, the absorption energy is calculated as the vertical energy difference between the ground and the absorbing excited state (in general a S_n excited state), both at the ground state

stable geometry (minimum energy structure). This geometry can be optimized computationally or obtained from experimental measurements. On the other hand, emission energies are calculated as the energy difference between the emitting excited state and the ground state, at the excited state structure (lowest energy geometry).

Kasha's rule states that emission only happens from the first excited state of each spin symmetry,[31] so emission will take place from the S_1 state species in case of fluorescence, or from the T_1 state structure in case of phosphorescence. If there are several minimum energy structures, the emission spectra can show more than one emission band, depending on the relative probability of population of the different minima that correspond to emitting species of different geometry and nature.

In general, after the initial excitation to the S_n state, a very fast non-radiative decay to S_1 takes place, and the system relaxes its geometry to reach the minimum energy structure of this state. But in many systems the lowest excited states is triplet (T_1), so an intersystem crossing from S_1 to T_1 can take place if spin-orbit coupling is large, characteristic favored by the well-known heavy atom effect. The system will then relax on the T_1 state populating the minimum (or minima) of this state. If the T_1/S_0 spin-orbit coupling is sizable, the system can decay actively giving place to phosphorescence. This is the case of systems with transition metal atoms, like the Cu system under study, where the large spin-obit coupling increases the probability of the non-radiative transition from S_1 to T_1 and the probability of radiative T_1-S_0 transitions, increasing the quantum yield of phosphorescence and decreasing the triplet lifetime.

Given that there is no experimental estimate of excited state geometries, we optimize the geometry of the lowest triplet excited state to obtain the geometry of the stable excited species responsible for the emission.

The main parameters of the lowest energy geometries of the S_0 ground state obtained with the cluster model and different density functionals are collected in Table 1. Comparison to the data extracted from the X-ray diffraction experiments on the Cu-Cy crystals [10], also in Table 1, show that the overall agreement is reasonable, especially for the parameters involving the atoms closest to the central Cu(1) atom (atom labelling is shown in Figure 3). The largest deviation is found for the Cu(2)-S(3) distance, for which none of the density functionals for the cluster model gives a correct description. The X-ray data show that Cu(2) forms stronger bonds with S(1), S(2) and N, but the interaction with S(3) is much weaker. This of course manifest the limitation of the cluster model considered here in calculating the bonds at the outer boundary of the cluster. The missing boundary condition of the system can be recovered by considering the extended system in periodic boundary conditions with appropriate Van der Waals correction for the Cu(2)-S(3) bond length. The last column of the Table 1 does show that the errors are systematically minimized for all the structural parameters with the periodic boundary condition calculations. For the cluster model, the functional that provides the best general agreement with experimental data are PBE0 (mean error 6.13%) and CAM-B3LYP (mean error 6.13%), while less accurate results are obtained with the B3LYP functional (mean error 8.69%). While with the periodic boundary condition, the largest error was 2%, which was for the Cu(2)-S(3) bond

length, with mean error less than 1%. Nevertheless, this discrepancy is not expected to significantly affect the absorption properties of the excited states localized in the region around Cu.

Table 1. DFT distances [Å], angles [°], dihedral angles [°] and errors relative to the crystallographic data (%) of the S_0 optimized geometry. The periodic model calculations considered the Van der Waals corrections to the GGA Hamiltonian.

	Exper.	Cluster model						Periodic model	
	X-ray	B3LYP	%Δ	CAM-B3LYP	%Δ	PBE0	%Δ	HSE06 (vdW)	%Δ
Cu(1)-Cl	2.274	2.242	1.4	2.221	2.3	2.225	2.2	2.273	0.0
Cu(1)-S(1)	2.247	2.325	3.5	2.331	3.7	2.322	3.3	2.216	1.4
Cu(2)-S(1)	2.285	2.273	0.5	2.271	0.6	2.264	0.9	2.260	1.1
Cu(2)-S(2)	2.317	2.290	1.2	2.279	1.6	2.281	1.6	2.300	0.7
Cu(2)-S(3)	2.611	3.410	30.6	3.115	19.3	3.024	15.8	2.559	2.0
Cu(2)-N	2.067	2.254	9.0	2.169	4.9	2.180	5.5	2.074	0.3
S(1)-Cu(1)-Cl	120.3	116.0	3.6	117.4	2.4	116.7	3.0	120.16	0.1
S(1)-Cu(1)-S(1)	119.5	128.0	7.1	125.2	4.8	126.6	5.9	119.68	0.2
Cu(2)-S(1)-Cu(1)	111.2	90.2	18.9	98.3	11.6	99.3	10.7	111.19	0.0

The geometries of the triplet species have been determined computationally as well. Using the cluster model a minimum energy structure has been located on the T_1 potential energy surface. Inspection of its electron density shows that the Cu ions in the cluster are best described by a $3d^{10}4s^0$ electronic configuration as expected for Cu^{1+} ions in a coordination compound.[10] As will be shown below in more detail, this triplet state is originated by the replacement of an electron from one of the 3d orbitals to a more diffuse Cu(4s)-like orbital in Cu(1) (labelling in Figure 3). In Table 2, we compare the results from the different density

functionals for the triplet structure; we list the changes in each parameter with respect to the corresponding parameters in the ground state optimized geometry of S_0. In this case it is not possible to compare the computed results with experimental data given that the triplet is too short-lived to perform X-ray diffraction experiments. The largest geometric changes that we observe in the relaxation of the T_1 states are connected to the Cu(2) ions, particularly the Cu(2)-S(3) and Cu(2)-N distances. These changes are not necessarily determinant for the emission properties because they involve atoms on the outside of the cluster that may not be directly involved in the radiative processes, but only provide an electrostatic background for the central part of the cluster.

Table 2. DFT distances [Å], angles [°] and dihedral angles [°] of the T_1 optimized geometry obtained using different functionals for the cluster model and changes with respect to the ground state geometry.

	Cluster model				Periodic model	
	B3LYP		CAM-B3LYP		HSE06 with vdW	
	DFT	$\Delta(S_0\text{-}T_1)$	DFT	$\Delta(S_0\text{-}T_1)$	DFT	$\Delta(S_0\text{-}T_1)$
Cu(1)-Cl	2.184	-0.058	2.153	-0.068	2.279	-0.006
Cu(1)-S(1)	2.328	0.003	2.289	-0.042	2.245	-0.029
Cu(2)-S(1)	2.313	0.040	2.300	0.029	2.282	-0.022
Cu(2)-S(2)	2.322	0.032	2.300	0.021	2.301	-0.001
Cu(2)-S(3)	3.121	-0.289	3.221	0.106	2.486	0.073
Cu(2)-N	2.116	-0.138	2.093	-0.076	2.119	-0.045
S(1)-Cu(1)-Cl	123.3	7.3	123.6	6.2	120.97	-0.81
S(1)-Cu(1)-S(1)	113.3	-14.7	112.9	-12.3	118.06	1.62
Cu(2)-S(1)-Cu(1)	104.5	14.3	104.0	5.7	112.66	-1.47

On the other hand, using the periodic model two different minima were located for T_1. By removing the symmetry restrictions of the C2/c space group that connect the Cu(1) atoms in the unit cell, we obtained a minimum T_1 structure with the two unpaired electrons localized in the region of one of the Cu(1) atoms. This structure is located 3.67 eV above the S_0 minimum and has been labelled as T_1 $Cu(1)_{no\text{-}sym}$ minimum. Only by keeping the full C2/c symmetry, which forces the spin density to be delocalized over the four equivalent Cu(2) centers, the geometry optimization finished with a new minimum on the T_1 surface, $Cu(2)_{sym}$, at 3.49 eV from the S_0 minimum. As expected the distortions are small in this case, whereas larger changes in the geometry are calculated for the $Cu(1)_{no\text{-}sym}$ minimum as can be seen in Table 3.

Table 3. DFT distances [Å] of the T_1 optimized geometries obtained using PBE0 functional for the periodic model and changes with respect to the ground state geometry.

	T_1 $Cu(1)_{no\text{-}sym}$ min				T_1 $Cu(2)_{sym}$ min	
		$\Delta(S_0\text{-}T_1)$		$\Delta(S_0\text{-}T_1)$		$\Delta(S_0\text{-}T_1)$
Cu(1)-Cl	2.268	-0.042	2.222	-0.088	2.322	-0.012
Cu(1)-S(1)	2.197	0.058	2.196	0.056	2.146	-0.006
Cu(2)-S(1)	2.176	0.012	2.009	-0.155	2.212	-0.048
Cu(2)-S(2)	2.180	-0.118	2.203	-0.095	2.294	0.005
Cu(2)-S(3)	2.965	0.246	2.983	0.264	2.644	0.075
Cu(2)-N	2.126	0.045	2.147	0.066	2.075	0.006

3.2 Character of the states involved in the transitions

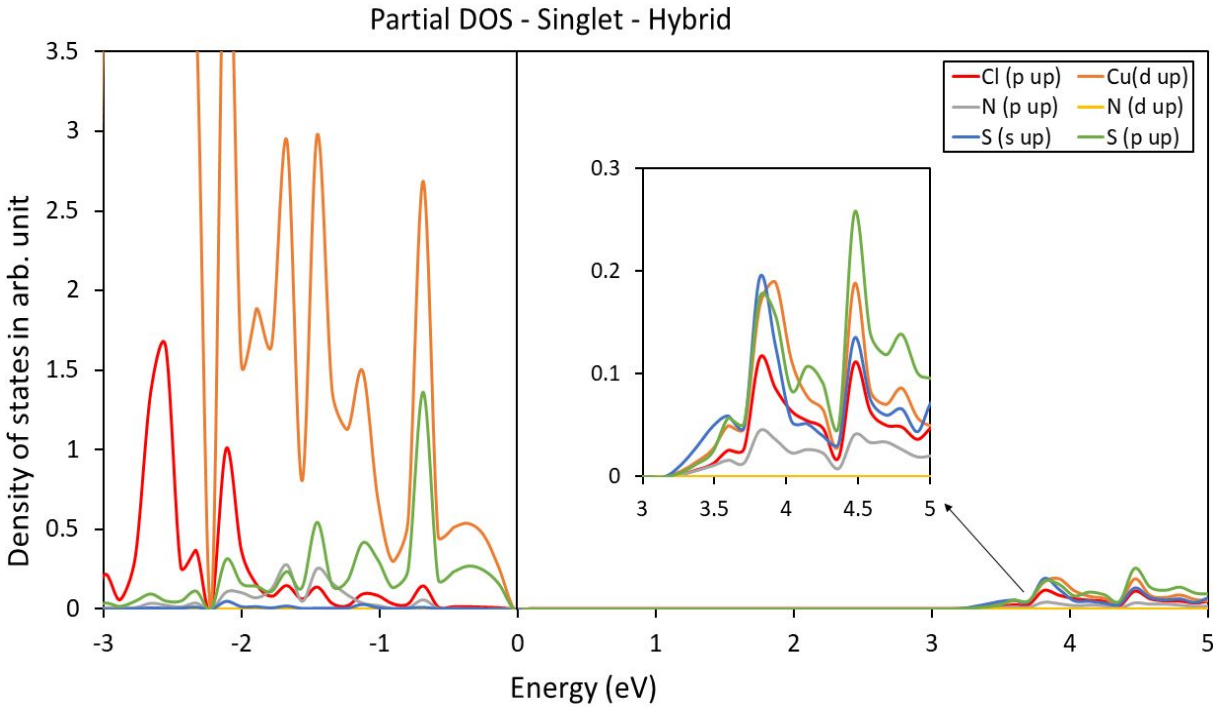

Figure 4: Orbital projected density of states (pDOS) plot for the S_0 Cu-Cy calculated with hybrid density functional theory (HSE06). The inset shows the amplified view of the conduction band pDOS. The top of the valence band is scaled to 0 eV, also called the Fermi level. Even though spin-polarized calculations were performed, as for S_0 states spin-up and spin-down states have exactly the same behavior, so spin-up DOS is plotted here.

To obtain a characterization of the orbitals participating in the absorption process, we have calculated the orbital projected partial density of states (pDOS) from the periodic calculations as shown in Figure 4. The valence band is mainly composed of Cu(1) 3d orbital and a significant contribution from S 2p orbital. At the conduction band minima, initially, S-2s orbital dominates, however, S-2p has almost equal contribution. This implies that S_0 to S_1 transition will be mainly initiated by Cu-3d to S-2p excitations, as p-d transitions has higher probability. Two points to note; first, the estimated bandgap from the DOS plot is about 3.21 eV, which is very close to the measured bandgap; second, there is a significant contribution from Cu-4s orbital near the conduction band minima. Thus, the presence of dominant Cu 3d (occupied) near the valence band and Cu-4s (unoccupied) near the conduction band does imply a $3d^{10}4s^0$ configuration of S_0 state, which is a Cu^{1+} oxidation state.

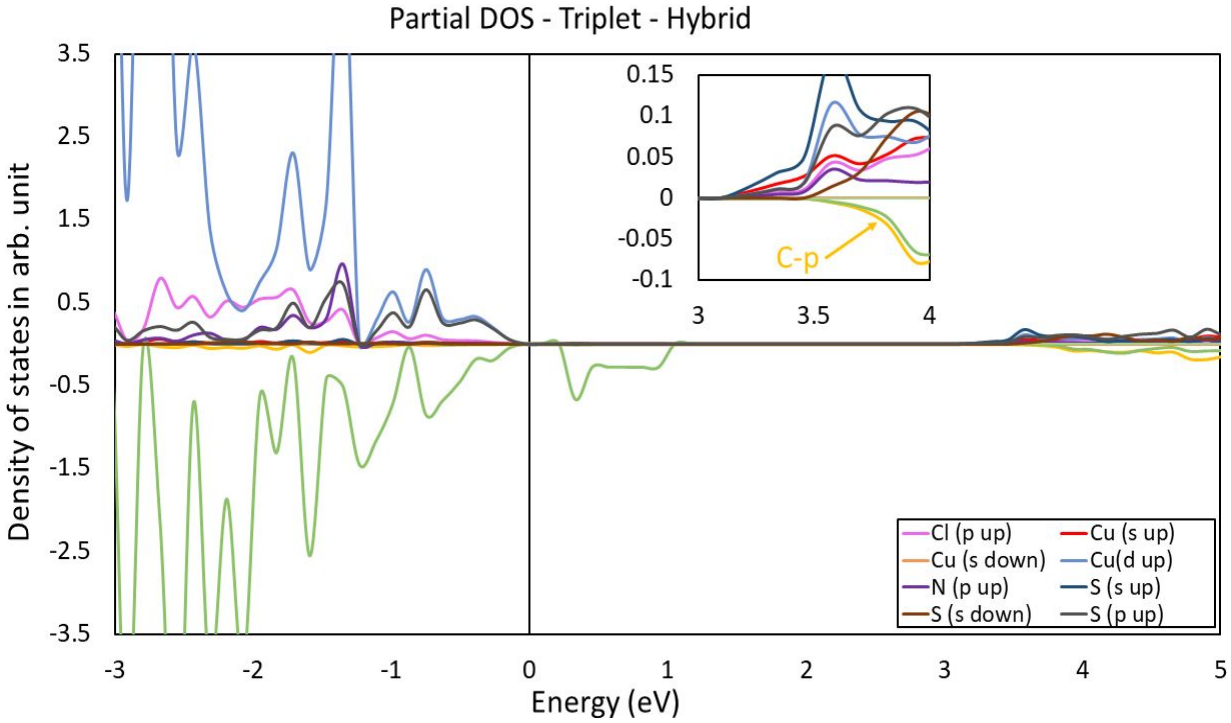

Figure 5: Orbital projected density of states plot (pDOS) for the T_1 Cu-Cy calculated with hybrid (HSE06) density functional theory. The inset shows the amplified view of the conduction band pDOS. The top of the valence band is scaled to 0 eV, also called the Fermi level. The positive and negative density of states here are for spin-up and spin-down channels respectively. The empty band above the valence band is from Cu-3d band, which was not found in S_0 state as presented in Figure 4.

Figure 5 shows the orbital projected density of states (pDOS) for the triplet T_1 state for Cu-Cy. To illustrate the spin-polarization, the spin-up and spin-down contributions are shown explicitly. From the pDOS several important points are to be noted here: (i) the lowest bandgap is 3.22 eV in the spin-up channel; (ii) the top of the valence band is still dominated by Cu-3d orbital with a mixture of S-2p orbitals; (iii) the presence of the empty band from Cu-3d orbital above the valence band which was absent in Figure 4; (iv) the presence of unoccupied Cu-s in spin-up conduction band and absence of it in the spin-down conduction band. These last two facts confirm that T_1 state has Cu $3d^9 4s^1$ configuration, which implies a Cu^{1+} oxidation state. The spatial extension of orbital 4s is larger than that of orbitals 3d, somewhat reflected in the bond lengths of S_0 (Cu $3d^{10}4s^0$) and T_1 (Cu $3d^9 4s^1$) Cu-cysteamines as presented in table 2.

Further understanding of the radiative processes in the Cu-Cy crystal can be obtained by analyzing the character of the electronic states involved in the absorption and emission. As mentioned before, the Cu(1) ion has a $3d^{10}4s^0$ character in the ground state and can be thought of as a Cu with oxidation state Cu^{1+}. Typical low-lying excitations with respect to this closed shell reference state involve metal to ligand charge transfer (MLCT), ligand to metal charge transfer (LMCT) or metal centered (MC) excitations. To start with, LMCT states can be excluded because reducing Cu^{1+} would require too much energy. On the contrary, the transfer of

a Cu-3d electron to the 4s orbital (MC excitation), or to an unoccupied ligand orbital (MLCT) are expected to be found at lower energy.

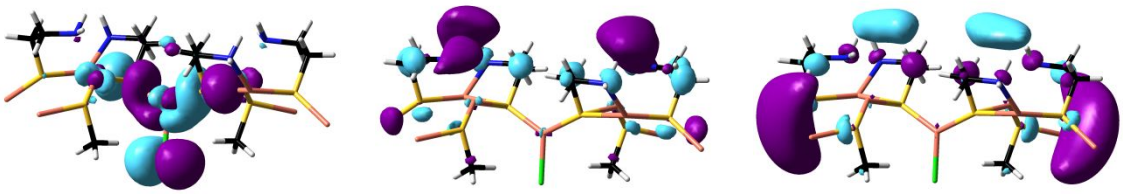

HOMO LUMO LUMO+2

Figure 6. Molecular orbitals involved in the excitation that gives place to the first excited singlet state.

The analysis of the TD-DFT results of the cluster model shows that the first excited state arises from 40% of the electron excitation from the highest occupied molecular orbital (HOMO in **Figure 6**) to the lowest unoccupied molecular orbital (LUMO in **Figure 6**), and the second largest contribution (HOMO to LUMO+2) only adds 1.1% to the total excitation. It means that more than 58% of the total excitations' character consist of various other very small contributions. The overall transitions we have here are between the S_0 and the S_1 (absorption), and the T_1 and S_0 (emission) states. The intermediate non-radiative transition from S_1 to T_1 state can be in part due to spin-orbit coupling, enhanced by the well-known heavy atom effect and often reported to be large for Cu^{+1} compounds (see for example ref. 32), and in part to the presence of defect states, such as Cu vacancies which are very probable in Cu^{+1} [33] compound that is in S_0 state. Furthermore, though there are fundamental boundary conditions different between the cluster and the periodic crystal calculation model, comparison of Figures 4 and 6 shows that the top of the valence band (or HOMO in cluster model) from where the electron excitation will take place is centered around the Cu(1) atoms. On the other hand, the excited state T_1 has also a valence band maximum centered at Cu(1). Of course, in both S_0 and T_1, Cu orbital atoms are hybridized with S-2p orbitals. However, due to the electronic distribution of Cu^{1+} in T_1 state ($3d^9 4s^1$), this state is catalytically more active compared to the ground state S_0 (with a $3d^{10}4s^0$ electron configuration Cu^{1+}). This directly correlate with the experimental fact that at the optical excitation Cu-cysteamine gets chemically activated.

Absorption and emission energies

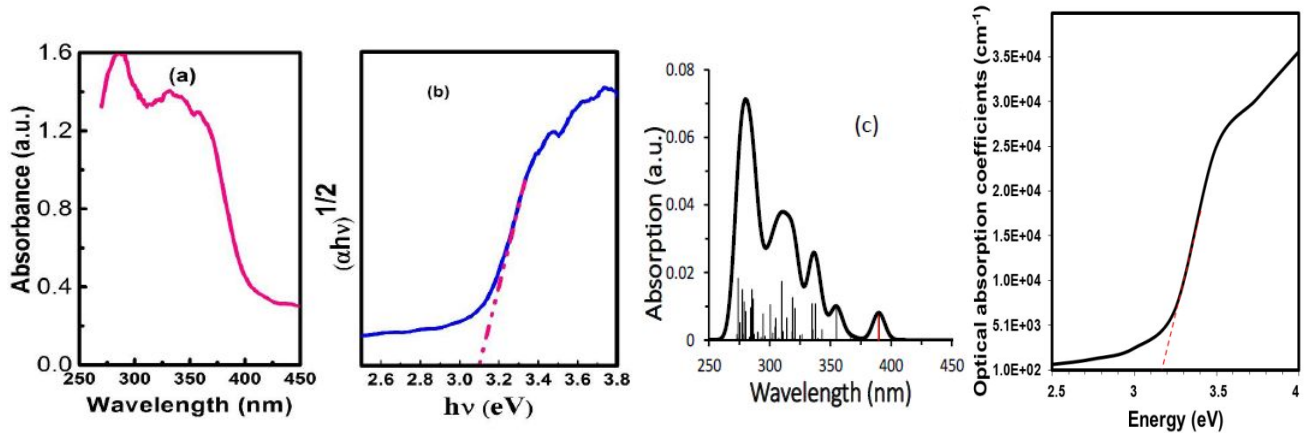

Figure 7. a) Experimental absorption spectrum of the Cu-Cy crystal. b) The plotting graph between $(\alpha h\nu)^{1/2}$ versus photon energy ($h\nu$). c) Computed absorption spectrum. The vertical lines corresponds to the calculated excitation energies, the red one is the S_0-S_1 transition. The solid line is the convolution with gaussians. d) Optical absorption coefficients calculated by the band structure calculations with periodic boundary conditions.

The experimental absorption spectrum of the Cu-Cy system (**Figure 7a**) shows a rise in the absorbance at 400 nm, which reaches a maximum at approximately 280 nm. The plotting graph between $(\alpha h\nu)^{1/2}$ versus photon energy ($h\nu$), the so called Tauc plot, is shown in **Figure 7b;** estimated optical bandgap is about 3.1 eV. Cu-Cy NPs have a first strong absorption in the UV range with a strong peak at about 365 nm but almost no absorption in the visible range, which makes Cu-Cy distinct from other photosensitizers like porphyrins which have strong absorptions in both UV and visible ranges.[34] The strong absorption in UV range makes it possible to combination with other UV sensors for treating bacteria or virus because UV is widely used for sterilization.The absence of absorption in visible makes it devoid of toxicity or side-effects under sunshine or room light, which has been a concern for photodynamic therapy on practical applications. [35, 36]

To reproduce the experimental absorption spectrum computationally, absorption energies are calculated as the energy difference between the ground state and the excited states at the ground state geometry. With the cluster model, excitation energies were obtained with TD-DFT for the first 50 singlet states; the energy lines were then convoluted with a gaussian type function, whose height corresponds to the oscillator strength of the transition, and the full-width at half maximum was chosen to be 5 nm. This gives us the simulated spectrum shown in **Figure 7 c**, where the red line corresponds to the S_0-S_1 transition. Note that only absorptions of energies up to approximately 273 nm have been reproduced computationally in **Figure 7c**. The overall shape of the computational and experimental spectra within the comparable range, between 273 and 390 nm are similar. Both show an isolated feature just below 390 nm and several overlapping features of similar intensity extending out to higher energies. The computed spectrum does not reproduce the marked

increase of the absorption at the high-energy end of the spectrum, because of the limited number of excited states that were calculated within the cluster model.

To further check the quality of our results, we have compared the maximum of the first absorption peak in the experimental spectrum (365 nm) of Cu-Cy crystal with the theoretical results obtained by different functionals for the S_0-S_1 transition. We do this both for the experimental X-ray structure and the computationally optimized structure. Our calculations indicate that the S_0-S_1 transition carries significant oscillator strength and can hence be held responsible for the absorption peak at lowest energy. Results in Table 4 show that, for this first absorption, the best agreement with experimental data was obtained with the PBE0 functional at the computational geometry and for the CAM-B3LYP functional using the X-ray geometry. Nevertheless, to be consistent within the results for emission, where computational geometries must be used (given the lack of experimental geometries for this excited state species), we must look for a balance between good description of both, absorption energy and ground state geometry. In this case, considering the absorption energies calculated at the computed geometries, PBE0 provides the best results within the cluster model.

Table 4. DFT relative energies in nm (eV) for the S_0-S_1 absorption and the T_1-S_0 emission of the Cu-Cy system. Computational results are compared to the maxima of the absorption and emission bands measured experimentally.

		S_0-S_1		T_1-S_0
		Computed geometry	X-ray geometry	Computed geometry
Cluster model	CAM-B3LYP	312 (3.98)	339 (3.66)	388 (3.19)
	B3LYP	402 (3.09)	508 (2.44)	456 (2.72)
	PBE0	390 (3.18)	444 (2.79)	445 (2.79)
Periodic model	HSE	356 (3.48)		571 (2.17)
	Experimental	365 (3.40)		607, 633 (2.04, 1.96)

In an attempt to reproduce the measured optical absorption plot in Figure 7 (b), we have calculated the optical absorption coefficients from the band structure calculations with periodic boundary conditions. This is shown in Figure 7(d). As mentioned earlier while discussing the pDOS plot in Figure 4, the bandgap we

obtained from the hybrid DFT calculation with HSE06 functional for Cu-Cy was 3.21 eV, and the calculated absorption coefficients features matche well with the experimental Tauc plot presented in Figure 7(b).

Regarding emission, the measured photoluminescence emission spectrum shows two different emission bands with maxima at 607 nm and 633 nm.[10, 37] These bands may be attributed to emissions from excited states involving the two different types of Cu atoms in the crystal, or inter-band emission within the respective spin-states, however these hypotheses have not been fully confirmed experimentally.

As explained before, the cluster model used in this study is only capable of predicting the emission from the excited state localized in the Cu(1) atom. To estimate the emission from this excited state, the energy difference between the lowest-energy triplet (T_1) and the ground state was calculated at the minimum energy structure of the T_1 as reported in Table 2. The spin-orbit coupling between the T_1 and S_0 states has been calculated at this geometry, yielding a value of 17.48 cm^{-1}, showing that the radiative emission is possible from this species, that will be responsible of the phosphorescence of this compound.

By calculating the energies with periodic boundary conditions, estimations of the emission can be made as well. As explained before, with this model two different minima on the T_1 potential energy surface were located, indicating that there exist two potential emissive species. By calculating the energy of the S_0 state at these geometries, an estimate of the emission could be made.

The vertical energy difference between T_1 and S_0 states at the $Cu(2)_{sym}$ minimum was found to be 356 nm (3.48eV), higher than the maximum of the second peak in the experimental spectrum. However, it must be noted that this second minimum was obtained maintaining the full C2/c symmetry, and hence, a delocalized triplet state was obtained in which only a small part of the geometry relaxation is accounted for. The calculated emission energy must be considered as an upper bound and a hypothetical full localization of the spin density around just one Cu(2) atom would cause larger geometry distortions (as in the T_1 $Cu(1)_{nosym}$ minimum) bringing the T_1 and S_0 much closer in energy. The vertical energy difference between the T_1 $Cu(1)_{no\text{-}sym}$ minimum and the ground state is 571 nm (2.17 eV), which is in good agreement with the maximum of one of the observed experimental bands. Note again that, with no-constraint full relaxation with periodic boundary condition, even with advanced hybrid function like HSE06 and corresponding starting structures, $Cu(2)_{sym}$ and $Cu(1)_{no\text{-}sym}$ structures cannot be stabilized distinguishably.

From the band structure calculations, we explain the transitions found as following: after the non-radiative transition from S_1 to T_1, the T_1 to S_0 emission can occur in two possible ways, a direct transition to T_1 to S_0 state; this emission is already mentioned above with a wavelength of 356 nm. To understand the second possibility, we need to refer to the pDOS plot of Figure 5. Note the bandgap for triplet Cu-Cy is 3.22 eV, which is very close to the gap of the singlet state. An excited electron in S_1 state will then experience a similar bandgap energy in T_1 state during the non-radiative transition. Now, this electron in T_1 excited state can de-excite to the first available lower energy which is the empty Cu 3d-band situated at an energy of 2.07

eV (599 nm) below the conduction band (Figure 5). This empty band has main contribution from the Cu(2) atoms in the spin down channel. However, as we have already discussed above that spin-orbit coupling will be significant here, spin will not be a conserved entity in optical transition, so this band will participate actively in the light emission process. This transition energy is very close to the 607-633 nm range. The width of the mid-gap state can give rise to the observed two-band emission.

Concluding Remarks

The Cu-cysteamine crystal has been represented by a cluster model and a periodic model to study the absorption and emission properties. To choose the appropriate density functional and to address the quality of the proposed material model, we compared the computed ground state geometries and absorption energies with experimental data. This comparison confirms that the model proposed is good enough to provide qualitative results, and that satisfactory quantitative results can be obtained with hybrid DFT functionals, namely PBE0 (cluster model) and HSE06 (periodic crystal model). For the periodic model, Van der Waals potential was added in the DFT Hamiltonian to accurately represent weak interlayer interactions. Using this computational set-up, we have also reproduced satisfactorily the absorption spectrum and absorption coefficients of the Cu-Cy compound.

In agreement with experimental assignments, from these computational results we conclude that the initial absorption leads the system to the S_1 state, then after non-radiative transitions, the emission takes place from the T_1 state. The electronic structure study of the initial and final states in the absorption and emission processes indicates that the nature of the excited states involved in these processes are mostly Cu-centered. Absorption corresponds to $3d^{10} \rightarrow 3d^9 4s^1$ configuration change on the Cu atom and the emission process to the inverse process deexciting radiatively the T_1(Cu $3d^9 4s^1$) electronic state to the S_0(Cu $3d^{10}$) state. The cluster model used allows an analysis of the nature of the excited states that involve excitations in the Cu(1) center, but unfortunately, it cannot be used to reproduce transitions involving the Cu(2) atom.

Alternatively, one can approach the problem from the periodic point of view. The unit cell contains two Cu(1) and four Cu(2) atoms, equivalent in the ground state, S_0, geometry. Like the cluster model, T_1 state is stabilized by the Cu-$3d^9 4s^1$ electronic configuration. However, unlike the cluster model, the optical absorption coefficients obtained from the periodic model compared well with the experimentally obtained one up to some high energy. Our periodic model results assigned approximately the two emission bands observed experimentally. One emission corresponds to the transition from T_1 to S_0 centered on the Cu(1) ion. The second emissions involving two bands at slightly lower energy is tentatively assigned to first de-excitation of T_1 state via mid-gap states to S_0, can involve mainly Cu(2) ion as well (about 600 nm).

Acknowledgements: We would like to acknowledge the support from the U.S. Army Medical Research Acquisition Activity (USAMRAA) under Contracts of W81XWH-10-1-0279 and W81XWH-10-1-0234 and partially the NIH/NCI 1R15CA199020-01A1. MNH is supported by National Science Foundation (USA)

award no. 1609811. This study is also supported by the National Natural Science Foundation of China (91222110).

References

1. R. A. Festa and D. J. Thiele, *Curr. Bio.*, 2011, **21**, R878.

2. H. Tapiero, D. M. Townsend and K. D. Tew, *Biomed Pharmacother* 2003, **57:386-398.**, 386-398.

3. S. Ishida, P. Andreux, C. Poitry-Yamate, J. Auwerx and D. Hanahan, *PNAS* 2013, **110**, 19507-19512.

4. R. G. Pearson, *J. Am. Chem. Soc.*, 1963, **85**, 3533.

5. c. Anshul Gupte a, Russell J. Mumper, *Cancer Treatment Reviews*, 2009, **35**, 32-46.

6. C. Santini, M. Pellei, V. Gandin, M. Porchia, F. Tisato and C. Marzano, *Chem. Rev.* , 2014, **114**, 815−862.

7. R. N. Patel, K. K. Shukla, A. Singh, M. Choudhary, U. K. Chauhan and S. Dwivedi, *Inorganica Chimica Acta*, 2009, **362**, 4891-4898.

8. A. Nasulewicz, A. Mazur and A. Opolski, *J.Trace Elements in Medicine and Biology* 2004, **18**, 1-8.

9. L. Finney, S. Vog, T. Fukai and D. Glesne, *Clin Exp Pharmacol Physiol*, 2008, **36**, 88-94.

10. L. Ma, W. Chen, G. Schatte, W. Wang, A. G. Joly, Y. Huang, R. Sammynaiken and M. Hossu, *J. Mater. Chem. C*, 2014, **2**, 4239-4246.

11. L. Ma, X. Zou and W. Chen, *J. Biomed. Nanotechnol.* , 2014, **10**, 1501-1508.

12. M. Yao, L. Ma, L. Li, J. Zhang, R. X. Lim, W. Chen and Y. Zhang, *J. Biomed. Nanotechnol.*, 2016, **12**, 1835–1851.

13. W. Chen and L. Ma, *US Patent* 2017, US 9,593,131 B592, March 514, 2017.

14. Z. Liu, L. Xiong, G. Ouyang, L. Ma, S. Sahi, K. Wang, L. Lin, H. Huang, X. Miao, W. Chen and Y. Wen, *Scientific Reports*, 2017, **7**, 9290.

15. X. Huang, F. Wan, L. Ma, J. B. Phan, R. X. Lim, C. Li, J. Chen, J. Deng, Y. Li, W. Chen and M. He, *CANCER BIOLOGY & THERAPY*, 2019, **20**, 812–825.

16. P. Wang, X. Wang, L. Ma, S. Sahi, L. Li, X. Wang, Q. Wang, Y. Chen, W. Chen and Q. Liu, *Part. Part. Syst. Charact.*, 2018, 1700378.

17. L. Shi, P. Liu, J. Wu, L. Ma, H. Zheng, M. P. Antosh, H. Zhang, B. Wang, W. Chen and X. Wang, *Nanomedicine doi.org/10.2217/nnm-2019-0094*, 2019.

18. S. Shrestha, J. Wu, B. Sah, A. Vanasse, L. N. Cooper, L. Ma, G. Li, H. Zhen, W. Chen and M. P. Antosh, *PNAS, 2019, 116, 16823*

19. L. Huang, L. Ma, W. Xuan, X. Zhen, H. Zheng, W. Chen and M. R. Hamblin, *J. Biomed. Nanotechnol.* 2019, 15, 2142

20. S. Hirata and M. Head-Gordon, *Chem. Phys. Lett.* , 1999, **314**, 291-299.

21. G. Kresse and D. Joubert, *Physical Review B*, 1999, **59**, 1758.

22. G. Kresse and J. Furthmuller, *Computational Materials Science*, 1996, **6**, 15-50.

23. M. J. Frisch, G. W. Trucks, H. B. Schlegel, G. E. Scuseria, M. A. Robb, J. R. Cheeseman, G. Scalmani, V. Barone, B. Mennucci and G. A. Petersson, *Gaussian, Inc.: Wallingford, CT, USA, 2009*.

24. T. Yanai, D. P. Tew and N. C. Handy, *Chem. Phys. Lett.* , 2004, **393**, 51-59.

25. A. D. Becke, *J. Chem. Phys.* , 1993, **98**, 1372–1377.

26. C. Adamo and V. Barone, *J. Chem. Phys.*, 1999, **110**, 6158-6170.

27. K. G and F. J, *Physical Review B*, 1996, **54**, 11169.

28. P. E. Blöchl, *Phys. Rev. B*, 1994, **50**, 17953.

29. J. Heyd, G. E. Scuseria and M. Ernzerhof, *The Journal of Chemical Physics*, 2006, **124**, 219906.

30. K. Berland, V. R. Cooper, K. Lee, E. Schroder, T. Thonhauser, P. Hyldgaard and B. I. Lundqvist, *Rep. Prog. Phys.* , 2015, **78**, 066501.

31. M. Kasha, *Disscussion of Faraday Society*, 1950, **9**, 14-19.

32. R. Enoki, H. Gamou, M. Kohda and J. Nitta, *Applied Physics Express*, 2018, **11**, 33001.

33. S. K. Barman and M. N. Huda, *J. Phys. Condens Matter*, 2018, **30**, 165701.

34. R. Bonnett, *Chemical Society Reviews*, 1995, **24**, 19.

35. T. F. Delaney and E. Glatstein, *Compr Ther*, 1988, **14**, 43-55.

36. H. I. Pass, *J Natl Cancer Inst*, 1993, **85**, 443-456.

37. H. Guo, J. Zhang, L. Ma, J. L. Chavez, L. Yin, H. Gao, Z. Tang and W. Chen, *Adv. Funct. Mater.* , 2015, **25**, 6833-6838.

A table of content:

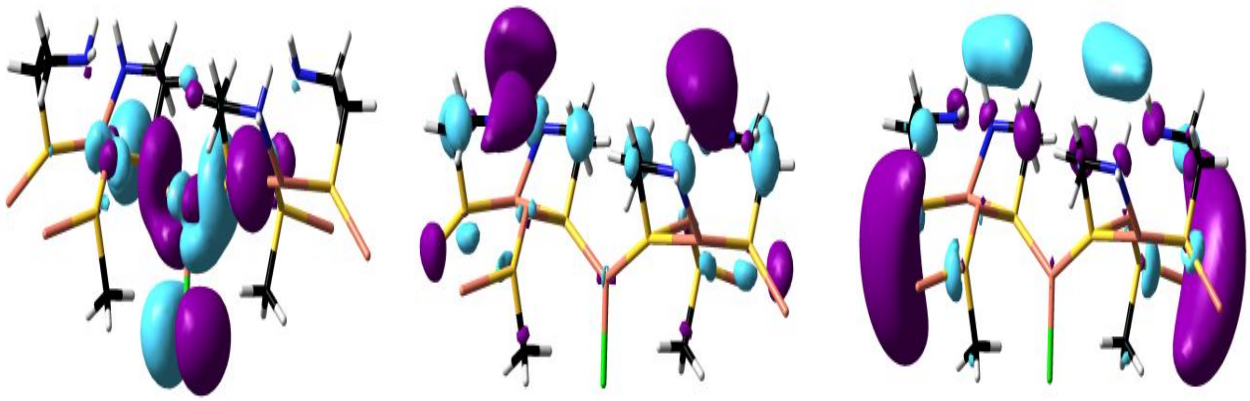

HOMO **LUMO** **LUMO+2**

A computational energy structures to illustrate the nature of the excited states involved in the photophysical processes of Copper Cysteamine